NASA

Technical Memorandum 85121

SATURN'S IONOSPHERE: INFERRED ELECTRON DENSITIES

M. L. Kaiser, M. D. Desch, and
J. E. P. Connerney

DECEMBER 1983

National Aeronautics and
Space Administration

Goddard Space Flight Center
Greenbelt, Maryland 20771

SATURN'S IONOSPHERE: INFERRED ELECTRON DENSITIES

M. L. Kaiser, M. D. Desch, and J. E. P. Connerney

Laboratory for Extraterrestrial Physics

Goddard Space Flight Center

Greenbelt, MD 20771

Accepted for publication by Journal of Geophysical Research

Abstract

During the two Voyager encounters with Saturn, radio bursts were detected which appear to have originated from atmospheric lightning storms. Although these bursts generally extended over frequencies from as low as 100 kHz to the upper detection limit of the instrument, 40 MHz, they often exhibited a sharp but variable low frequency cutoff below which bursts were not detected. We interpret the variable low-frequency extent of these bursts to be due to the refraction and reflection of the radio waves as they propagate through an ionosphere which varies with local time. We obtain estimates of electron densities at a variety of latitude and local time locations. These compare well with the dawn and dusk densities measured by the Pioneer 11 and Voyager Radio Science investigations, and with model predictions for dayside densities. However, we infer a two order-of-magnitude diurnal variation of electron density, which had not been anticipated by theoretical models of Saturn's ionosphere, and an equally dramatic extinction of ionospheric electron density by Saturn's rings.

Introduction

The Planetary Radio Astronomy (PRA) instrument onboard the two Voyager spacecraft detected a bursty, broadband emission originating from Saturn [Warwick et al., 1981, 1982]. These radio bursts, called SED for Saturn Electrostatic Discharges, were organized in episodes lasting several hours and separated from each other by about 10h 10m, distinctly less than the 10h 39.4m Saturn rotation period. Initial analyses [Warwick et al., 1981, 1982; Evans et al., 1981, 1982] suggested that the SED were generated by an unknown object in the rings of Saturn, where the Keplerian revolution period equals 10h 10m. However, this interpretation was questioned by Burns et al. [1983] who suggested instead that the bursts were the radio manifestations of atmospheric lightning storms. They pointed out that high-speed jets in the equatorial atmosphere would cause the cloud tops to super-rotate about every 10h 10m. Kaiser et al. [1983] demonstrated that a source in the rings could not produce the observed occurrence pattern of the SED but an extended source region in the equatorial atmosphere could account for the pattern. They also showed that the radio burst episodes often had a low frequency cutoff which they attributed to the refraction of lightning-generated radio waves away from the Voyager spacecraft as they propagated through Saturn's ionosphere.

In this paper, we examine in detail the low-frequency cutoff in the Saturn lightning burst data and construct a partial map of

the inferred ionospheric electron density as a function of latitude and local time.

Observations

Figure 1 shows examples of dynamic spectra recorded by the PRA instrument on Voyager-1. The PRA receiver operates in two bands; the high band extends from 40.5 to 1.5 MHz in 128 channels, and the low band extends from 1.3 MHz to 1.2 kHz in 70 channels. The receiver sweeps through all 198 channels every six seconds, spending a total of 30 msec on each individual channel. The dynamic spectra of Fig. 1 each contain 600 6-sec sweeps coded so that increasing darkness is proportional to increasing intensity. The dark band centered below 500 kHz is Saturnian kilometric radiation [see Warwick et al., 1981], a strong radio emission of magnetospheric origin, not of interest here. The short, vertical streaks are the radio bursts originating from atmospheric lightning. Even though it is believed that these bursts have a very broad bandwidth [Warwick et al., 1981], they appear as short streaks because of the receiver sampling scheme. Only the few frequency channels being sampled during the ~50 msec duration of a burst actually record the emission.

It is evident from Fig. 1 that, on some occasions, there is a frequency below which the lightning bursts are not observed. In panel a, bursts are not detected below about 5 MHz, whereas in panel b, the bursts are clearly present across the entire

instrument bandwidth. Panel c appears to show a cutoff frequency intermediate between panels a and b.

We believe these highly variable low-frequency cutoffs are related to the local time of the source and the spacecraft-Saturn encounter geometry. The latter is shown in figure 2 where the Voyager 1 flyby trajectory is projected onto the Saturnian globe. During the long period of time preceding the encounter, Voyager-1 was essentially fixed in Saturn's sky near the equator and near local noon, depicted by the black box in the left-hand panel. During the few-hour interval immediately surrounding closest approach (C.A.), Voyager-1 rapidly swung through a large angle in latitude and local time. The spacecraft then exited the Saturn system at the relatively fixed position of $+26^{\circ}$ latitude and 3.5 hr local time, shown by the black box in the right-hand panel.

Panel a of Fig. 1 was obtained during the inbound portion of the trajectory, when Voyager-1 was near the noon meridian as shown in Fig. 2. Panel b of Fig. 1 which showed lightning bursts to very low frequencies was obtained near Voyager-1 closest approach, when the spacecraft was near its most southerly latitude and midway between the dusk terminator and midnight. Panel c of Fig. 1 was obtained when Voyager-1 was over the night hemisphere of Saturn, near the outbound box shown in Fig. 2.

The low-frequency cutoffs can be used to compute a partial map of the ionospheric electron density provided we have some knowledge

of the storm location as a function of time. For Voyager-1, Kaiser et al. [1983] deduced that the storm stretched along the equator from 210° to 270° in the Saturn longitude system [see Desch and Kaiser, 1980] at the epoch 15h 10m on day 317 of 1980. Using this initial storm position and the 10h 10m storm system rotation rate, we can compute the location of the storm throughout the Voyager-1 encounter. For Voyager-2, the storm position is not nearly as well defined because of the decline in the number and intensity of SEDs [Kaiser et al., 1983]. While we have used only the Voyager-1 data set in our quantitative analysis, the Voyager-2 observations are qualitatively consistent with the results of our analysis of Voyager-1 data.

We have determined representative low frequency cutoffs from PRA dynamic spectra (like those in Fig. 1) for the three SED episodes centered on closest approach. During these episodes, the occurrence rate of SED was high enough to permit reliable measurements to be made. Table 1 lists the time and position of Voyager-1 near the beginning, middle and end of the three episodes. Also listed is the mean local time of the source region for that portion of the source visible to the spacecraft. The final column gives the observed low-frequency cutoff.

We note that Burs et al., [1983] proposed a different mechanism for obtaining a depletion of ionospheric electron density. They suggested that the shadow of the rings would block solar EUV, creating a low density band around Saturn's equatorial zone

through which the low frequency SED could escape. However, Kaiser et al., [1983] showed that the low frequency SED were observed only on the nightside of the planet. The Burns et al. mechanism should lead to escape of low frequency SED on the dayside as well. There is no evidence at present to support the Burns et al. hypothesis.

Analysis Technique

Using the data from Table 1 and assuming that the low frequency cutoff is due to ionospheric propagation effects, we have performed a ray tracing analysis in order to determine the maximum electron density along the propagation path between Voyager-1 and the storm complex. We have used the three-dimensional ray tracing program developed by Jones and Stephenson [1975] for a birefringent medium with appropriate replacement of the earth's ionosphere and magnetic field by those of Saturn. We have used the collision-free Appleton-Hartree refractive index equations.

We assume for convenience in ray tracing that the Saturnian ionosphere can be approximated by an ideal Chapman layer, with a peak density altitude of 1100 km above the 1 bar level, and a 300 km scale height [see Waite, 1981], independent of solar zenith angle. The results are relatively insensitive to the assumed ionospheric altitude and scale height so the peak electron density alone was varied. The "Z_3" model magnetic field

[Connerney et al., 1982] was used and all rays were traced from an initial altitude of 0 km, at the 1 bar level in the atmosphere. This corresponds approximately to the NH_3 cloud level in Saturn's atmosphere. The NH_4SH and H_2O cloud levels are only ~ 80 km and ~170 km below the 1 bar level. Presumably the lightning discharges originate in association with precipitation at one of these atmospheric levels. It has been implicitly assumed that any cosmic ray induced ionosphere that may exist [Capone et al., 1977] is below the level where the SED originate, otherwise escape of emission below about 1 MHz would not be possible.

Figure 3 shows the result of a sample ray tracing exercise in which three rays at different frequencies have been launched into a model ionosphere as described above. For the case shown, the peak density was 10^4 cm^{-3}, and the rays have frequencies of 1.0, 1.2, and 1.5 MHz. All rays in this example were launched in the plane of the equator and at an elevation above the local horizontal of 30^o. (In the figure, the elevation angles of the rays are shown offset from each other for clarity.) The 1.0 MHz ray suffers a complete reflection in the ionosphere and so does not escape. The lowest frequency able to escape is 1.2 MHz, and this ray suffers some refraction as evident in the figure. This is the critical ray. The 1.5 MHz ray escapes easily. In our analysis, the peak ionosphere electron density is adjusted until the frequency of the critical ray matches the observed low frequency cutoff from Table 1. Propagation effects are

particularly significant when Voyager-1 observes the storm rising and setting. When the storm system appears at the local meridian and propagation occurs at nearly normal incidence, such effects are minimal.

Results

In Figure 4 we show the results of applying the ray tracing analysis to the data of Table 1. The densities plotted are the equatorial values as a function of a 24-hour local time clock in which 12 hr corresponds to local noon. Ordinate error bars are derived from the maximum and minimum densities obtained from the ray tracing, given the finite longitudinal extent (abscissa error bars) of the SED source visible to the spacecraft at the times noted in Table 1. Uncertainties in the measurement of the low-frequency cutoff are difficult to estimate because of the relative scarcity of SED events and are not included in the error estimates. Numbers assigned to each density observation are keyed to the observation numbers in the table.

There is a strong variation of the equatorial density with local time. The mean nightside density (average of observations 9,10,11 13,14) is about 2×10^3 cm^{-3}, and the mean dayside density (average of observations 1,2,4,5) is about 3×10^5 cm^{-3}, yielding a mean day-night density ratio of about 150. Observations numbered 3,12, and 15 overlap the dusk and dawn terminators on Saturn. The average of these values is about 4×10^4 cm^{-3}, intermediate between

the dayside and nightside extremes. The data, which suggest a sine wave dependence with local time, were least-squares fit to an equation of the form

$$\log n_e = A - B \cos(L.T. - \phi)$$

where n_e is the electron density, L.T. is the local time and ϕ is the phase shift. The fit (dashed line) shows that the peak-to-peak day-night change is about a factor of 450. This fit also reveals that the curve is phase shifted about the noon-midnight meridian by 0.80 hr towards dusk.

The results shown in Figure 4 pertain to sub-spacecraft latitudes that are near-equatorial. For these observations the spacecraft latitude never exceeded $\pm 28^{\circ}$, and we consider the variations in density to be due to changes in the source local time alone. Observations numbered 6,7, and 8, however, were made at greater southerly latitudes and the inferred densities were anomalously low. Observations 6 and 7, for example, at local times of 14.8 and 17.5 hr, yielded peak equatorial electron concentrations of 5×10^3 and 1.5×10^3 cm^{-3}, respectively, and observation 8 would require densities of less than 100 cm^{-3} over portions of the night hemisphere. These values are thus a factor of about 100 to 200 below those expected on the basis of the local time least-squares fit of Figure 4.

Discussion

Our analysis shows that Saturn's ionosphere appears to undergo a

strong diurnal variation, reaching a maximum equatorial density near local noon and a minimum density near midnight. The mean dayside equatorial density, 3×10^5 cm^{-3}, is in excellent agreement with models of Saturn's ionosphere. Virtually all of the models prior to the Pioneer-11 and Voyager encounters [see Atreya et al., 1984 and references therein] predicted a maximum density of about 2×10^5 cm^{-3}. The values we obtain at the dawn and dusk meridians are in good agreement with the equatorial dawn and dusk densities determined by the Pioneer-11 radio science team [Kliore et al., 1980], and in generally good agreement with the density values obtained at much higher latitudes by the Voyager radio science team [Tyler et al., 1981,1982].

We observe typical day-night variations in equatorial density of at least a factor of 100, and there appear to be other regions on the nightside where the density must fall to less than 100 cm^{-3}. By comparison, the earth exhibits a pronounced diurnal variation in electron density with typical day-night ratios of 10 to 100 in peak density [see Bauer, 1973 and references therein]. In the models of Saturn's ionosphere [Atreya et al., 1984], diurnal variations are assumed to be slight because the recombination time constant for H^+ is very long compared to Saturn's rotation (H^+ is assumed to be the major ionospheric ion species). However, Waite [1981] suggested that the dawn-dusk difference in the altitude of peak density observed by the Pioneer-11 spacecraft [Kliore et al., 1980] might be resolved by a diurnal variation in the altitude of the ionosphere. He further speculated that if the

altitude variation were large enough, at low altitudes H^+ would combine readily with atmospheric CH_4, greatly reducing the ionospheric density.

Our explanation for the observation of anomalous low frequency bursts near Voyager-1 closest approach (observations 6, 7 and 8) invokes a drastically reduced ionospheric profile at high southern latitudes and multihop propagation. In this scheme, low frequency rays originating near the equator are reflected between the bottom of the solar EUV ionosphere and the top of the cosmic ray ionosphere until they reach a point where the electron density of the EUV ionosphere permits escape. Many reflections are possible before significant loss of wave energy occurs because the total wave absorption due to electron-ion collisions within the ionosphere is only about 0.1 dB per reflection [see e.g., Radcliffe, 1962] if the electron temperature is 1000 K [Atreya et al., 1983]. A schematic of this geometry is shown in Figure 5. These anomalous low frequency events all occurred at the southernmost extremity of Voyager-1's closest approach, between dusk and midnight. The multihop propagation proposed to explain these events requires a reduction of the ionospheric electron density at latitudes between -23° and -39° to ~1 or 2 % of the equatorial electron density at the same local time (i.e. Fig. 4). These are latitudes that are magnetically connected to the rings, as illustrated in Figure 5. Using the Z_3 model magnetic field, -39° latitude maps to the inner edge of the B ring (see Table 2), and -23° maps just inside the inner edge of

the C ring. The remainder of the Voyager-1 trajectory was spent at latitudes equatorward of those linking the ionosphere with the rings. We speculate that the inferred ionospheric extinction occurs as well in the Northern hemisphere at appropriate conjugate latitudes listed in Table 2.

Reduction of the ionospheric electron density at these latitudes to 1 to 2% of the equatorial density implies that the rings are either an extremely effective sink for ionospheric plasma or a source of ions which mix with and deplete the ionospheric population [Atreya and Donahue, 1975; Waite, 1981] with equal efficiency. Note that observations 4 and 5 (Table 1) occur at -25° and -28°, respectively, but do not show evidence of the ionospheric extinction exhibited by observation 8 which extends down to -23° latitude. Observations 4 and 5 occur over the sunlit hemisphere at a latitude linked magnetically through the tenuous C ring. Observation 8 occurs over the night hemisphere. We speculate that the extinction due to interaction with the C ring is small or comparable to the solar EUV production rate, and hence is not detectable in these observations over the dayside hemisphere.

Over the night hemisphere, however, in the absence of the EUV production, the C ring sink can effectively and quickly reduce the ionospheric density by ~2 orders of magnitude. At higher latitudes, where magnetic field lines link through the optically thick B ring, some extinction is evident in observations 6, 7,

and 8 over both the sunlit and night hemispheres. We speculate that the extinction due to the interaction of the B ring with the ionosphere can compete with the EUV production rate, resulting in a reduction in ionospheric density at these latitudes over the entire planet.

Northrop and Hill's work [1983] on the stability of high charge-to-mass ratio particles in Saturn's ring plane provides a mechanism for ion transport to the ionosphere. They found that high charge-to-mass ratio dust particles or ions created at any radius inside of either the inner edge of the B ring (1.52 R_S) or 1.62 R_S (depending on the particle's magnetic moment) would be unstable in the equatorial plane and would precipitate into Saturn's ionosphere.

We can roughly estimate the total mass from the rings required to partially neutralize the ionosphere in the B-ring magnetic footprint. If we assume that the flow of material from the inner B-ring can neutralize an electron density of $\sim 10^4$ cm^{-3} in about one hour (corresponding to the inferred falloff near the dusk terminator), then the flow rate must be about 3×10^{27} ions/sec over the footprint area. If the principle material is OH as suggested by Shimizu [1980], this would correspond to about 75 kg/sec. Over the lifetime of the ring system, this flow would be comparable to the present mass of the inner part of the B-ring, and could thus be responsible for the observed large decrease in optical depth observed in the B-ring inward of 1.64 R_S.

The very low inferred electron densities at these latitudes would result in a similarly low ionospheric electrical conductivity. This, in turn, may influence a wide range of upper atmospheric and magnetospheric phenomena on a planetary scale. Reduced conductivity at latitudes linked via field lines with the rings may, for example, allow large radial electric fields in the B ring, a possibility mentioned in connection with the formation of spokes [Warwick et al., 1981].

Acknowledgement The authors are deeply indebted to J.H. Waite, Jr., J.K. Alexander, Jr., and T.J. Birmingham for many helpful comments and suggestions.

Table 1

EPSD. #	OBS. #	DOY	DATE 1980	VOYAGER LAT	VOYAGER L.T. (hr)	STORM MEAN L.T. (hr)	LF CUTOFF (MHz)
1	1	317	12 NOV 0900	-02	13.6	9.0 (r)	8.6
	2	"	" 1200	-04	13.8	14.2 (t)	3.7
	3	"	" 1425	-07	14.0	18.3 (s)	6.5
2	4	317	12 NOV 2030	-25	15.6	11.8 (r)	18.0
	5	"	" 2100	-28	16.0	12.6 (")	10.0
	6	"	" 2210	-37	17.3	14.8 (")	1.0
	7	"	" 2320	-39	19.7	17.5 (")	0.5
	8a	317	12 NOV 2345 through	-39	20.6	18.4 (t)	0.1
	8b	318	13 NOV 0120	-23	23.5	22.0 (")	0.1
	9	"	" 0140	-19	23.9	22.4 (")	0.3
	10	"	" 0330	-04	1.1	2.6 (s)	0.5
	11	"	" 0500	+03	1.7	5.2 (")	1.0
	12	"	" 0600	+06	1.9	6.0 (")	4.0
3	13	318	" 1040	+13	2.5	22.0 (r)	0.6
	14	"	" 1300	+16	2.7	1.3 (t)	0.4
	15	"	" 1600	+17	2.9	6.8 (s)	1.3

r=source rising
t=source transiting
s=source setting

Table 2

Z_3 CONJUGATE LATITUDES

RING	R_S	LATITUDE NORTH	LATITUDE SOUTH
D (inner)	1.11	27°	-17°
C (inner)	1.23	35	-26
B (inner)	1.52	44	-38
(outer)	1.95	52	-47
A (inner)	2.02	53	-48
(outer)	2.27	55	-51

References

Atreya, S.K. and T.M. Donahue, Ionospheric models of Saturn, Uranus and Neptune, Icarus, 24, 358-362, 1975.

Atreya, S.K., J.H. Waite, Jr., T.M. Donahue, A.F. Nagy, and J.C. McConnell, Theory, measurements, and models of the upper atmosphere and ionosphere of Saturn, In Saturn, ed. T. Gehrels and M. Mathews, U. of Arizona Press, Tucson, in press, 1984.

Bauer, S.J., Physics of Planetary Ionospheres, Springer-Verlag, New York, 1975

Burns, J.A., M.R. Showalter, J.N. Cuzzi, and R.H. Durisen, Saturn's electrostatic discharges: could lightning be the cause?, Icarus 54, 280-295, 1983.

Capone, L. A., R. C. Whitten, S. S. Prasad, and J. Dubach, The ionospheres of Saturn, Uranus, and Neptune, Astrophy. J., 215, 977-983, 1977.

Connerney, J.E.P, N.F. Ness, and M.H. Acuna, Zonal harmonic model of Saturn's magnetic field from Voyager 1 and 2 observations, Nature, 298, 44-46, 1982.

Desch, M.D. and M.L. Kaiser, Voyager measurement of the rotation period of Saturn's magnetic field, Geophys. Res. Lett., 8,

253-256, 1981.

Evans, D.R., J.W. Warwick, J.B. Pearce, T.D. Carr, and J.J. Schauble, Impulsive radio discharges near Saturn, Nature, 29, 716-718, 1981.

Evans, D.R., J.H. Romig, C.W. Hord, K.E. Simmons, J.W. Warwick and A.L. Lane, The source of Saturn electrostatic discharges, Nature, 299, 236-237, 1982.

Jones, R.M. and J.J. Stephenson, A versatile three-dimensional ray tracing computer program for radio waves in the ionosphere, U.S. Dept. of Commerce report # 75-76, 1975.

Kaiser, M.L., J.E.P. Connerney, and M.D. Desch, Atmospheric storm explanation of Saturnian electrostatic discharges, Nature, 303, 50-53, 1983.

Kliore, A.J., I.R. Patel, G.F. Lindal, D.N. Sweetnam, H.B. Hotz, J.H. Waite, Jr., and T.R. McDonough, Structure of the ionosphere and atmosphere of Saturn from Pioneer 11 Saturn raio occultation, J. Geophys. Res., 85, 5857-5870, 1980.

Northrop, T.G. and J.R. Hill, The inner edge of Saturn's B ring, J. Geophys. Res., 88, 6102-6108, 1983.

Radcliffe, J.A., The Magnetoionic Theory, Cambridge University

Press, Cambridge, 1962.

Shimizu, M., Strong interaction between the ring system and the ionosphere of Saturn, Moon Planets, 22, 521-522, 1980.

Tyler, G.L., V.R. Eshleman, J.D. Anderson, G.S. Levy, G.F. Lindal, G.E. Wood, and T.A. Croft, Radio science investigations of the Saturn system with Voyager 1: preliminary results, Science, 212, 201-206, 1981.

Tyler, G.L., V.R. Eshleman, J.D. Anderson, G.S. Levy, G.F. Lindal, G.E. Wood, and T.A. Croft, Radio science with Voyager 2 at Saturn: atmosphere and ionosphere and the masses of Mimas, Tethys, and Iapetus, Science, 215, 553-558, 1982.

Waite, J.H., Jr., The ionosphere of Saturn, Ph.D. dissertation, University of Michigan, 1981.

Warwick, J.W., J.B. Pearce, D.R. Evans, T.D. Carr, J.J. Schauble, J.K. Alexander, M.L. Kaiser, M.D. Desch, B.M. Pedersen, A. Lecacheux, G. Daigne, A. Boischot, and C.W. Barrow, Planetary radio astronomy observations from Voyager 1 near Saturn, Science, 212, 239-243, 1981.

Warwick, J.W., J.B. Pearce, D.R. Evans, J.H. Romig, J.K. Alexander, M.D. Desch, M.L. Kaiser, M. Aubier, Y. Leblanc, A. Lecacheux, and B.M. Pedersen, Planetary radio astronomy

observations from Voyager 2 near Saturn, Science, 215, 582-587, 1982.

Figure Captions

Figure 1. Three 1-hour dynamic spectrograms of the highest resolution data from the Voyager-1 PRA instrument. Increases in intensity above the PRA receiver threshold are indicated by increases in pixel darkness. The SED are the short vertical streaks. The gray variable background evident in the PRA high band is spacecraft-generated noise. In the low band is the radio emission which emanates from Saturn's magnetosphere known as Saturnian kilometric radiation. In panel a, the SED are not detected below about 5 MHz, whereas in panel b, they appear throughout the entire frequency range. In panel c, the SED are observed down to about 0.5 MHz.

Figure 2. The trajectory of Voyager-1 projected onto the disk of Saturn. The sub-Voyager track remains nearly fixed in Saturn latitude and local time during the long inbound and outbound portions of the trajectory. Only during the few hours near closest approach does the spacecraft show significant motion in latitude and local time. Tic marks along the trajectory are in hours on Nov. 12-13, 1980.

Figure 3. A schematic ray tracing exercise. Three rays of different frequency are launched in the equator plane from a point 1100 km below the altitude of peak density (10^4 cm^{-3}) in the ionosphere. The lowest frequency escaping is 1.2 MHz. The initial elevation angle of all three rays is 30° (offset here for

clarity).

Figure 4. The equatorial electron concentrations as a function of local time. Maximum and minimum concentrations occur just after noon and midnight, respectively as indicated by the least-squares fit to the data (dashed curve).

Figure 5. Encounter trajectories of Voyager-1 and -2 in a cylindrical coordinate system aligned with Saturn's spin axis, and a schematic of the multihop ionospheric propagation to escape at high latitudes. Z_3 model field lines threading the inner and outer extremities of the B ring are illustrated. Positions of Voyager-1 during observations labelled 5 through 8 in Table 1 are indicated as well as latitudes linking the ring features. The lightning flash, shown slightly above the equator for clarity, indicates the point of origin of the radio emission in Saturn's atmosphere.

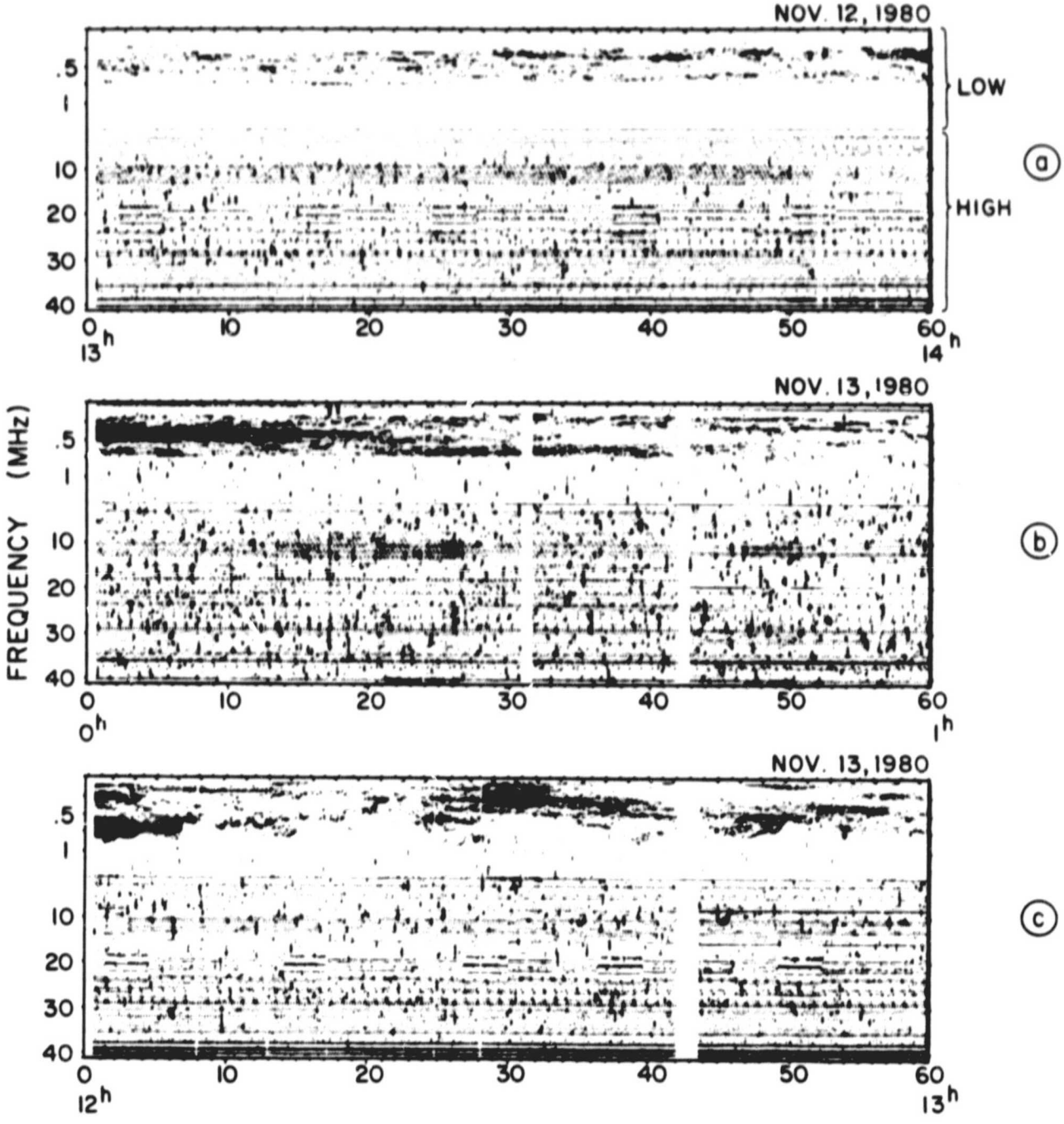

Figure 1

Figure 2

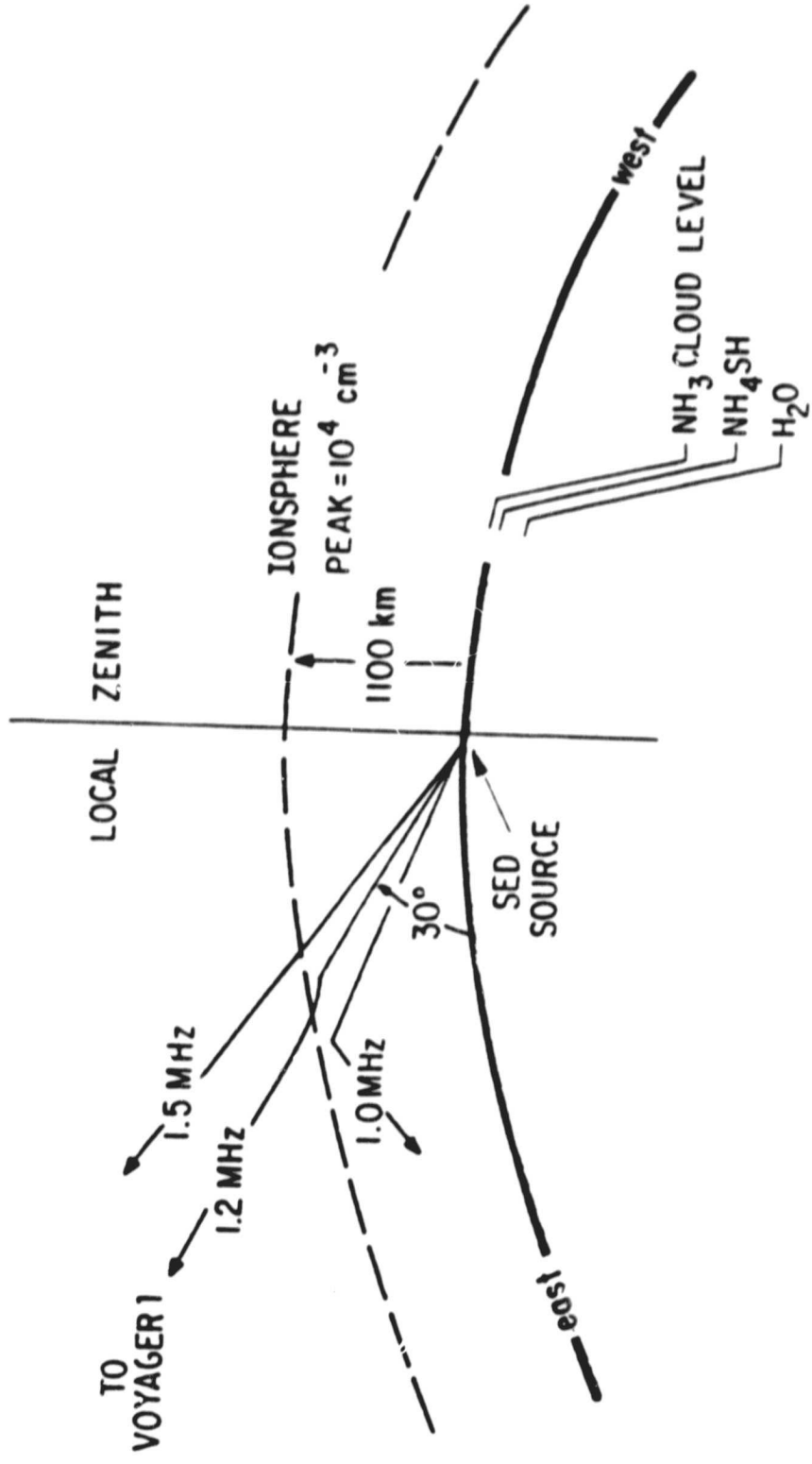

Figure 3

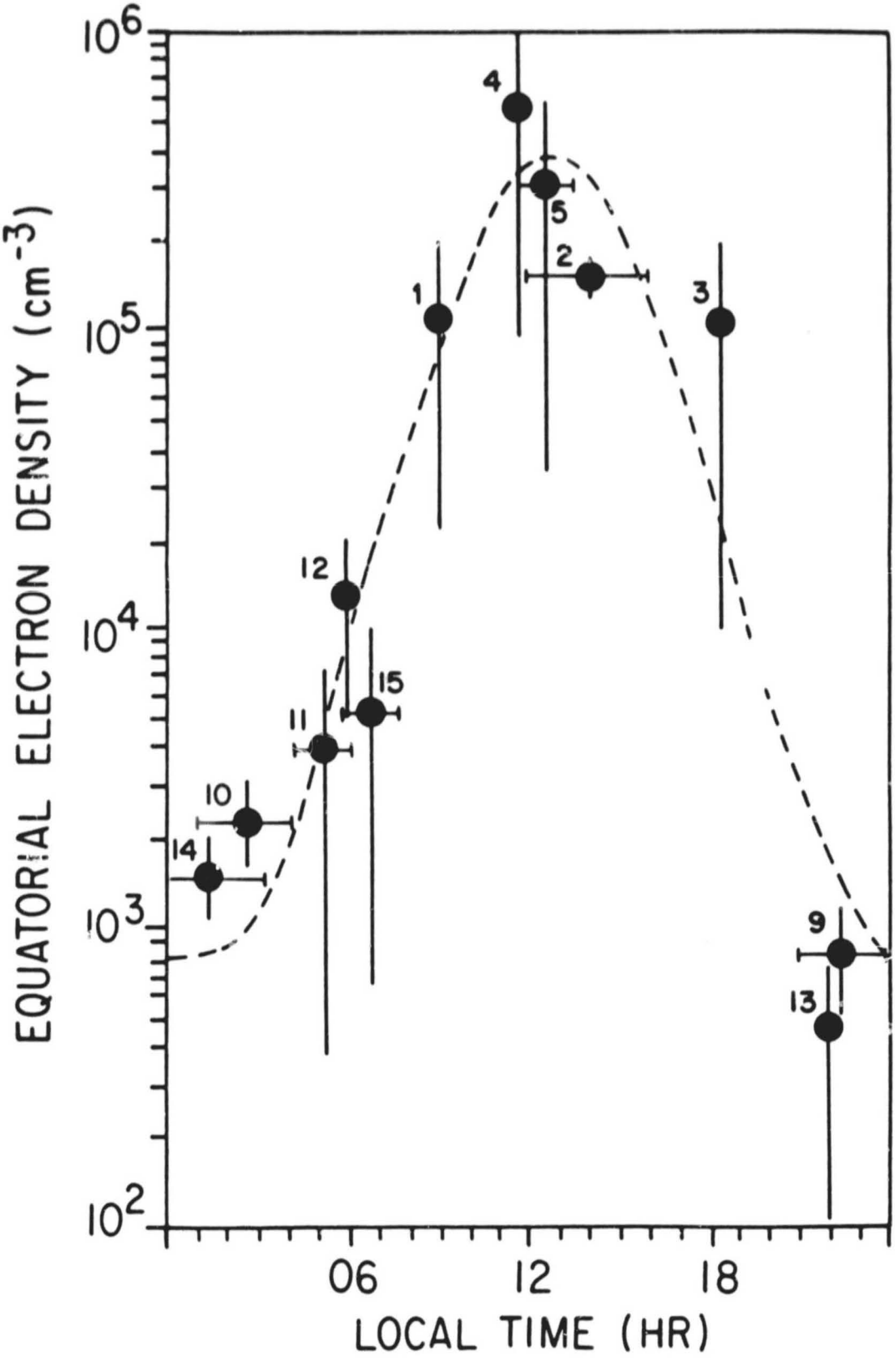

Figure 4

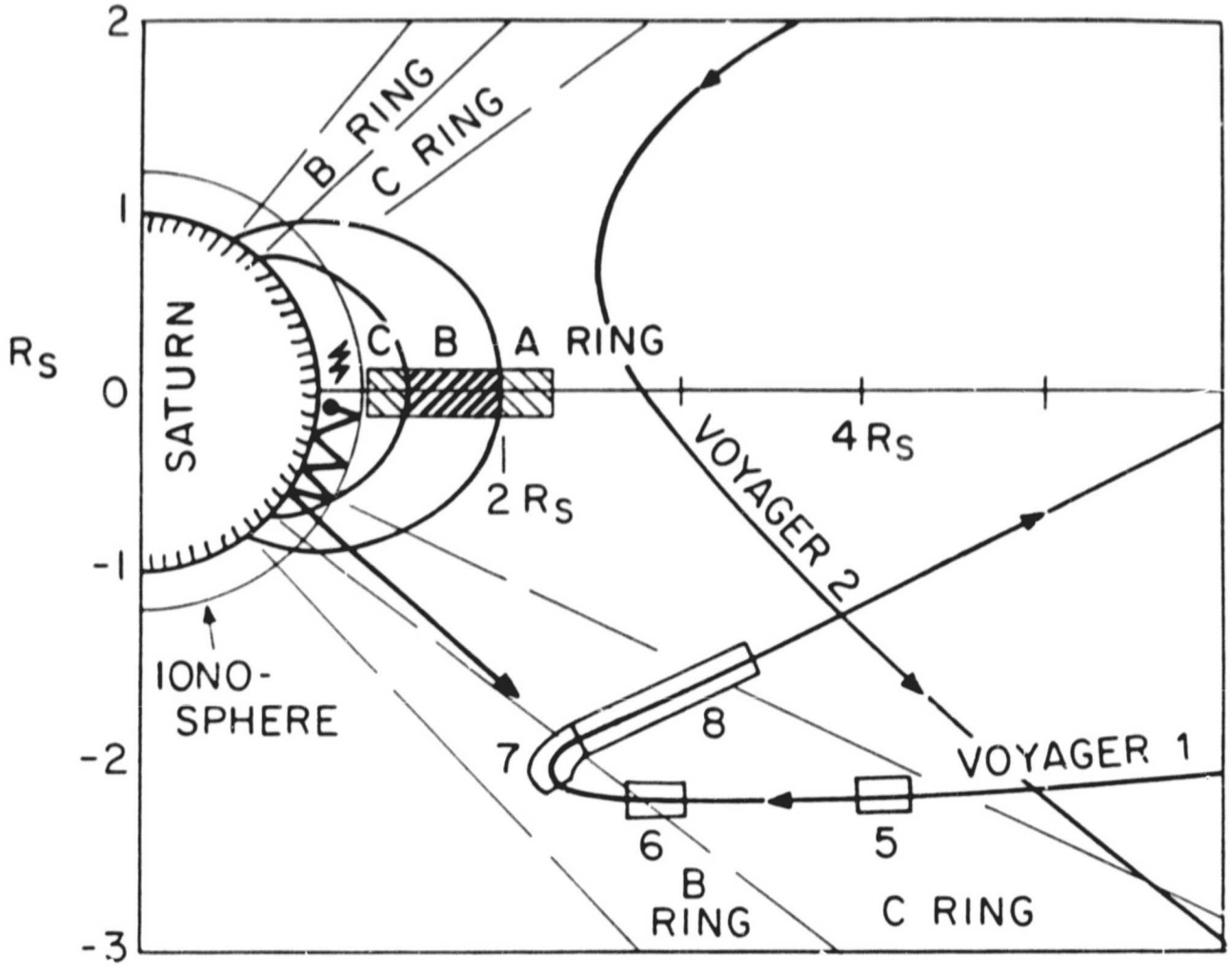

Figure 5